



Effect of spaces between aligned tubes having a semicircular section on heat exchange attributes

T.M. Almulla, M.W. Shawki, M.F. Abd Rabbo, Y.A. Al-Mashad, M.R. Salem

Mechanical Engineering Department, Faculty of Engineering at Shoubra, Benha University, Shoubra ,Cairo, Egypt

Abstract : This paper introduces experimental tests to investigate the hydrothermal characteristics of align-complete circular tube (CCT) or semicircular tube (SCT) banks at a wide range of airflow across the tubes. The tests considered several gap ratios between the bases ($0.126 \leq \delta \leq 0.378$) of pairs of SCTs with different pitch ratios in transversal/longitudinal directions. The findings declare that the SCT is a helpful passive tool for supplementing the air-cooling load, while it also leads to raising the airflow resistance, when compared with systematic shape. Moreover, the \overline{Nu}_o and f_o are increased by expanding the space between the flat bases and decreasing the spacing between the tubes in both directions. Besides, the hydrothermal performance approach (HTPA) is affected by varying SCT geometrical parameters. It is increased by increasing the gap between the flat SCTs-bases in addition to the transversal pitch and decreasing the longitudinal pitch. It is recorded that the maximum value of HTPA through this study is 2.25.

Keywords: Inline setting; Semi-circular cross section; Spaces; Performance

Nomenclatures

A Area, m²
 Cp Specific heat, J/kg . °C
 d Diameter, m
 f Fanning friction factor
 h Convection heat transfer coefficient, W/m² . °C
 k Thermal conductivity, W/m . °C
 L Length, m
 ṁ Mass flow rate, kg/s
 P Pressure, Pa
 Q Heat transfer rate, W
 S Gap between the bases of two adjacent SCTs, m
 T Temperature, °C or K
 u Velocity, m/s
 Ṃ Volume flow rate, m³/s

Dimensionless groups

\overline{Nu} Average Nusselt number
 Pr Prandtl number
 Re Reynolds number
 St Stanton number

Greek letters

α Attack angle, °

β Temperature ratio
 Δ Differential
 δ Base gap ratio
 δ Gap ratio
 γ Heat capacity ratio
 μ Dynamic viscosity, kg/m . s
 ρ Density, kg/m³

Superscripts and subscripts

ave Average
 b Base
 c Cross-sectional
 cir Circular
 h Hydraulic
 i Inner or inlet or internal
 LM Logarithmic Mean
 m Mean
 max Maximum
 o Out or outer
 s Surface
 t Tube

Acronyms and abbreviations

CCT Complete Circular Tube
 HTPA Hydrothermal Performance Approach
 SCT Semi-Circular Tube

1. Introduction

Tube banks in crossflow are well-thought-out one of the well-known types of heat exchange tools that are employed in several industries as in steam producers and air coolers. Moreover, the aligned/staggered bundle is usually branded by the tube diameter and by the transversal and longitudinal pitches. The flow and thermal attributes of this type of heat exchanger are very vital to be judged. Thus, rising the exchange rate more than that in usual practice will improve the effectiveness in such submissions besides their capital and operating expenses [1, 2].

There is a great history of research on the behaviour of tube banks' performance. Baughn et al. [3] performed experimental runs on the heat exchange from isofluxed CCT bundle. The authors assured that for both in-line and staggered CCT arrangements, the heat exchange coefficient could be recognized by the third row. Zhang et al. [4] accomplished tests on the effect of the spacing of in-line vortex generators on the heat/mass transmissions through finned flatten tube bank. The authors recorded that the optimal spacing hinges on the performance assessment principle. Moawed [5] observed the performance of an in-line tube bundle of single SCTs. The study considered isofluxed conditions. Nada et al. [6] studied the flow/heat transfer of an airflow across single isofluxed SCT at different attack angles. Bayat et al. [7] accomplished a study using a cam-shaped staggered CCT bank. It was documented that the pressure decay was 92-93% smaller than the CCTs. Zhao et al. [8] numerically simulated the heat transfer from finned oval tubes combined with dimples and/or vortex generators. He et al. [9] simulated the sedimentation of sulfuric acid on an H-type finned CCT bank. The findings assured that the fin thickness and flow velocity have the highest effect on acid sedimentation.

Yilmaz and Yilmaz [10] studied the effects of different dimensions of in-line isothermal CCT bank on its thermal performance. Yilmaz et al. [11] numerically simulated the thermal action of axially finned inline CCT configuration. The results recorded that the fins augmented the heat exchange at a lower pressure drop. Martinez- Wang and Cheng [12] simulated the attributes of air crossing a rotated aligned tube bank. Compared to the original design, the results recorded maximum reductions in the pressure drop and total cost by 69.7% and 16.3%, respectively. Mohanan et al. [13] numerically simulated the airflow patterns around CCT and flattened staggered tube bundles of five rows. It was reported that employing elliptic tubes attained higher performance than employing mixed (elliptic and circular) and circular tubes, respectively. Ramírez-Hernández et al. [14] carried out tests on the thermal action of an airflow crossing CCTs under frost formation settings. The authors observed a non-uniform frost development at lower Reynolds numbers. Souza et al. [15] simulated the performance response of an

evaporator tube bundle of seven rows and different transverse pitches. Choudhary et al. [16] practically outlined the effect of integrating perforated splitter plates to isofluxed tube bundle on the hydrothermal performance. It was recorded that the splitter plates augmented the thermal performance response. Zhong et al. [17] considered the condensation heat exchange on a bundle of in-line and staggered CCTs. From the introduced review, it is clear that there is no employed pair of SCTs instead of CCTs, which is considered a passive method to enhancing the exchange rate, especially that applying passive approaches avoids the need to the external power as active ones consume to accomplish the heat exchange augmentation [18-24]. The current experimental work judges the heat load and flow resistance across in-line pairs (Fig. 1) of CCT or SCT bank. The tests consider several gap ratios between the bases of pairs of SCTs with different pitch ratios in transversal/longitudinal directions. A dimensionless parameter, expresses the ratio between the SCTs spacing and the tube outer diameter, is the gap ratio (δ), defined as follows;

$$\delta = \frac{S_b}{d_{t,o}} \quad (1)$$

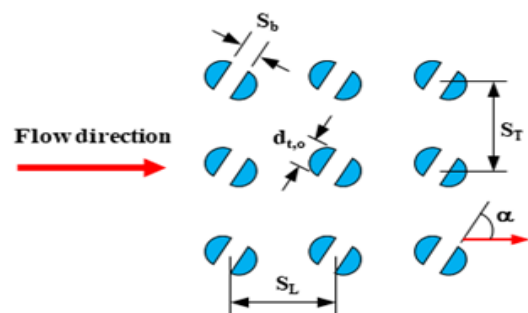


Fig. 1: Inline SCT bank.

2. Experimental Apparatus

In this investigation, the apparatus contains cooling water and heating air streams. The airflow line is an open-cycle, which incorporates a blower (5 hp, suction-type), air damper, orifice plate meter, transition duct, pressure devices, testing segment in which tube bundle is located, entrance channel, straightener, and air heater. The cooling water is a closed-loop, which involves a cooling system, pump, flow meter, valves, two headers, the tested inline tube bundle, and the piping. Fig. 2 represent outlines of the testing rig. The path of the airflow in the current device begins from the inlet channel, where there is an electric heater (6 kW) and a straightener package. Heater operation is specified via a pre-set thermostat to preserve a persistent temperature of the heating air crossing the bundle. The passageway is made of galvanized steel with dimensions of 950 x 250 x 3500 mm. The outer body is thermally insulated with glass wool. Then the air flows through the test portion

(at a distance of 2000 mm). There are two openings on the vertical sides of the tunnel (dimensions of 250 x 300 mm) in which two headers are installed. Then the air enters the measuring channel through the transitional part (convergent section). The flow rate measuring channel consists of two series of PVC pipe, manhole panel and downstream PVC pipe. 5HP-blower is used to preserve the air in the system. The air flowrate is controlled by an airflow retarder. The refrigeration unit consists of an insulated cabinet with a capacity of 100 liters. Heat is delivered from the water in the cabinet by two cooling units with a refrigeration load of 20 kW. The operation of the unit is based on a pre-set temperature regulator.

A 3 HP pump is used to circulate the water. Tested bundles consist of 20 CCTs or 40 SCTs; number of rows is $N_L = 5$ while number of columns perpendicular to the airflow is $N_T = 4$. The tubes are made of copper material with a diameter of 14.45 and 15.88 mm on the inside and outside, respectively, with a total length of 1000 mm for each. To form SCTs, the CCT is cut longitudinally through the plasma cutter. Next, a sheet of the same material, length, diameter, and thickness is welded lengthwise.

The tubes are organized as an in-line configuration with different spacing ratios in both the longitudinal and transversal directions. Furthermore, for the banks of SCTs, different gaps between the tube bases are considered. The attack angle of the bases of the SCTs is maintained at 60° . The characteristic dimensions of the different configurations are revealed in Table 1. Two tanks are incorporated in the present apparatus to meet the arriving water to/from the tubes. Two nipples are welded on both ends of each header. One end of each header is bolted to a blind flange to close off these ends, while the other ends are bolted to the nipple of the air duct. Totally, 32 rectangular housing dies (Fig. 3) are made of wooden sheets of dimensions of $320 \times 270 \text{ mm}^2$ (4 mm thickness) are sandwiched between the header and air duct nipples. The dies are drilled via a laser cut machine to provide holes of the same dimensions and number of the tubes. Additionally, ingoing and exit ports are soldered to both headers. The CCTs/SCTs are coupled with the two headers through the dies, taking into consideration to close off the space between the tubes and their holes.

Table 1: Distinguishing sizes of the tested tubes.

No.	α ($^\circ$)	S_b (mm)	δ	S_T (mm)	$S_T/d_{t,o}$	S_L (mm)	$S_L/d_{t,o}$
Tube bank of CCTs							
1		—		31.75	2.0	31.75	2.0
Tube banks of SCTs							
2 to 16	60	2, 4, 6	0.126, 0.252, 0.378	31.75	2.0	31.75	2.0
				39.69	2.5		
				47.63	3.0		
				47.63	3.0	31.75	2.0
						39.69	2.5
						47.63	3.0



Fig. 3: The rectangular housing-die

Variable zone flow meter, 10-100 L/min, flow rate range and reading accuracy $\pm 5\%$, is coupled to evaluate the water flowing rate. The airflow rate is estimated by measuring the pressure decay via a

digital pressure gauge; 0.001-69 kPa pressure difference range and accuracy of $\pm 1 \text{ Pa}$. The same instrument is also used to judge the pressure decay across a tube bank. Eight K-thermocouples are used to evaluate the inlet and outlet temperatures of both streams. Six of them are inserted directly into the airflow stream at the inlet and out of the test section, in three evenly spaced positions.

3. Experimental Procedures

To start experiments, air blower, air gate control unit, orifice plate meter, transition canal, test section, inlet duct, straightening device, heater, tube bundle, headers, chiller, pump, flow meter, thermocouples and differential pressure gauge are gathered. The cooling tank is filled with water, and then the blower, cooler, heater and pump are engaged.

Table 2: Testing circumstances.

Parameters/operating conditions	Range or Value
Air-side	
Airflow rate, m ³ /s	0.285–1.677 (1645 ≤ Re _{o,max} ≤ 12850)
Inlet temperature, °C	50±1 (Pr _o = 0.71)
Water-side	
Total water flow rate, l/min	61.2 (Re _i ≈ 3259)
Inlet temperature, °C	15 (Pr _i ≈ 7.94)

Fluid's inlet temperatures are controlled on both sides by adapting the temperatures of both the heater and coolant reservoir through their thermostats. The water flowing rate is estimated by the meter and valve fitting. While the air flowing rate is controlled via the damper. While conducting the experiment, it is assumed that the steady state at a maximum change of 0.5°C can be recorded within 25 min.

4. Heat Exchange and Flow Resistance Estimation

Firstly, the properties of both fluids; heating air and cooling water, are evaluated at their mean temperatures, $T_{a,m}$ and $T_{w,m}$, respectively. Then, the heat load rates on the air/water sides (Q_o and Q_i) are calculated. These are used to assess the heat load as there is a small difference between them due to measurement errors; max. deviation presented here is ± 4.4%.

$$T_{a,m} = \left(\frac{\sum T_{a,i}}{3} + \frac{\sum T_{a,o}}{3} \right) / 2 \quad (2)$$

$$T_{w,m} = (T_{w,i} + T_{w,o}) / 2 \quad (3)$$

$$Q_o = \dot{m}_o C p_o (T_{a,ave,i} - T_{a,ave,o}) \quad (3)$$

$$Q_i = \dot{m}_i C p_i (T_{w,o} - T_{w,i}) \quad (4)$$

The total thermal conductance is assessed using Eq. (5).

$$U_o A_{t,o} = \frac{Q_{ave}}{F \Delta T_{L,M}} \quad (5)$$

$$\Delta T_{L,M} = \frac{(\Delta T_i - \Delta T_o)}{\ln \left[\frac{\Delta T_i}{\Delta T_o} \right]} = \frac{(T_{t,i} - T_{sh,o}) - (T_{t,o} - T_{sh,i})}{\ln \left[\frac{T_{t,i} - T_{sh,o}}{T_{t,o} - T_{sh,i}} \right]} \quad (6)$$

$$F = \frac{\ln \left(\frac{1-\gamma\beta}{1-\beta} \right)}{(\gamma-1) * \ln \left[1 + \frac{\ln(1-\gamma\beta)}{\gamma} \right]} \quad (7)$$

$$\beta = \frac{T_{w,o} - T_{w,i}}{T_{a,ave,i} - T_{w,i}} \quad (8)$$

$$\gamma = \frac{T_{a,ave,i} - T_{a,ave,o}}{T_{w,o} - T_{w,i}} \quad (9)$$

γ and β are heat capacity and temperature ratios [25]. For the bundle walls, the fouling/conduction thermal resistances are omitted. So, the convection resistances are only incorporated to evaluate the overall coefficient;

$$\frac{1}{U_o A_{t,o}} = \frac{1}{h_o A_{t,o}} + \frac{1}{h_i A_{t,i}} \quad (10)$$

In Eq. (10), A_t is the surface area of the tubes, valued as follows;

$$A_t = 20\pi d_t L_t \quad \text{For CCTs} \quad (11)$$

$$A_t = 40d_t L_t (0.5\pi + 1) \quad \text{For SCTs} \quad (12)$$

Water flow through the tubes is quite turbulent with the ratio between tube length to hydraulic diameter of 65.7 for CCTs and 107.6 for SCTs, which is greater than 10. Thus, the average Nusselt number for the water side (\overline{Nu}_i) using the Gnielinski [26] correlation, Eq. (13);

$$\overline{Nu}_i = \frac{\frac{f_i}{2}(Re_i - 1000)Pr_i}{1 + 12.7\sqrt{\frac{f_i}{2}}(Pr_i^{2/3} - 1)} \left[1 + \left(\frac{d_{t,h}}{L_t} \right)^{2/3} \right] \quad (13)$$

Filonenko [27], Eq. (14) is utilized to get the f_i in Eq. (13).

$$f_i = 0.25(1.82 \log Re_i - 1.64)^{-2} \quad (14)$$

Then the average coefficient of transferred heat in the waterside is found as follows;

$$\bar{h}_i = \frac{\overline{Nu}_i \cdot k_i}{d_{t,h}} \quad (15)$$

In Eq. (16), $d_{t,h}$ is the tube hydraulic diameter, found as follows;

$$d_{t,h} = d_{t,i} \quad \text{For CCTs} \quad (16)$$

$$d_{t,h} = \frac{\pi d_{t,i}}{\pi + 2} \quad \text{For SCTs} \quad (17)$$

For the air-side, average Nusselt number (\overline{Nu}_o), can be assessed as follows;

$$\overline{Nu}_o = \frac{\bar{h}_o d_{t,o}}{k_o} \quad (18)$$

The water-Reynolds number is valued as;

$$Re_i = \frac{4\dot{m}_{i,tube}}{\pi d_{t,h} \mu_i} \quad (19)$$

The air velocity measured in the blank test section is called the surface velocity (u_o), which is obtained from the calibrated aperture meter. However, the interstitial velocity ($u_{o,max}$) depends on the free distances between tubes in each row; computed from;

$$u_{o,max} = \frac{u_o S_T}{S_T - d_{t,o}} \quad (20)$$

The interstitial velocity is used to determine the pattern of airflow through the tube bank by calculating the Reynolds and Stanton maximum numbers as follows;

$$Re_{o,max} = \frac{u_{o,max} d_{t,o}}{\nu_o} \quad (21)$$

$$St_o = \frac{\overline{Nu}_o}{Re_{o,max} \cdot Pr_o} \quad (22)$$

The air pressure drop (ΔP_o) is incorporated to assess Fanning friction factor for the air-side (f_o) as follows [28];

$$f_o = \frac{\Delta P_o}{2 N_L \rho_o u_{o,max}^2} \quad (23)$$

Moreover, for all runs, the uncertainties in the main variables/parameters do not exceed 5.4% (Appendix A).

5 Apparatus validation/outputs verification

The verification of the output of this study is done by comparing the recoded friction coefficients and heat exchange of the airflow with that resulted by Zukauskas [28], Eq. (24) and Jakob [29], Eq. (25) at the same operational conditions for aligned CCT bank. The documented data recorded a maximum difference 6.9%.

$$\overline{Nu}_o = 0.2484 Re_{o,max}^{0.63} Pr_o^{0.36} \tag{24}$$

$$f_o = \left[0.044 + \frac{0.08 * \frac{S_L}{d_{t,o}}}{\left(\frac{S_T}{d_{t,o}} - 1 \right)^{\left(0.43 + \frac{1.13 d_{t,o}}{S_L} \right)}} \right] Re_{o,max}^{-0.15} \tag{25}$$

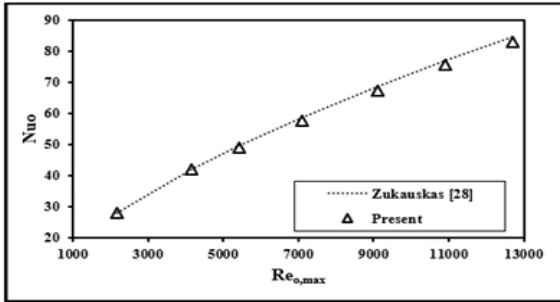


Fig. 4: Outputs of the \overline{Nu}_o verification assessments.

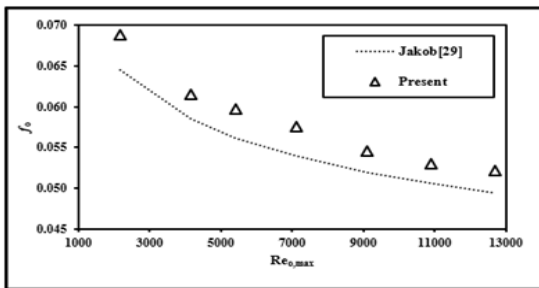


Fig. 5: Outputs of the f_o verification assessments.

6. Results and Discussions

6.1 Effect of Bases-Gap

This section presents the effect of splitting the tubes. Three different gaps between the SCTs-bases are considered, which form three gap/tube outer diameter ratios between 0.126 and 0.378. Fig. 6 demonstrates a sample of the recorded outputs for \overline{Nu}_o and f_o for the considered gap ratios at different airflow rates. It is noticeable that splitting the CCTs to pairs of SCTs raises both the cooling rate and pressure decay for the air. Besides, the increases in heat transfer rates and the pumping power are increased by increasing the gap between the SCTs-bases. Compared to the CCT bundle, the average percentage increases in \overline{Nu}_o and f_o are 56.2% and 24.5%, respectively, at $\delta = 0.126$. The corresponding increases at $\delta = 0.378$ are 66.5% and 30%, respectively. These results can be backed to two reasons. The first is increasing the heat transfer surface area by splitting the tube; the area increases from $20\pi d_{t,o} L_t$ for CCTs to $20\pi d_{t,o} L_t + 40d_{t,o} L_t$ for SCTs. The second reason is that increasing the gap between the flat bases of pair of SCTs throttles the main stream between the tube columns, which increases the disturbance of the air, and consequently improves the commingle between the fluid layers, which breaks the thermal and velocity boundary layers of the air-side flow. These augment the heat transfer rate and increase the flow pressure loss concurrently.

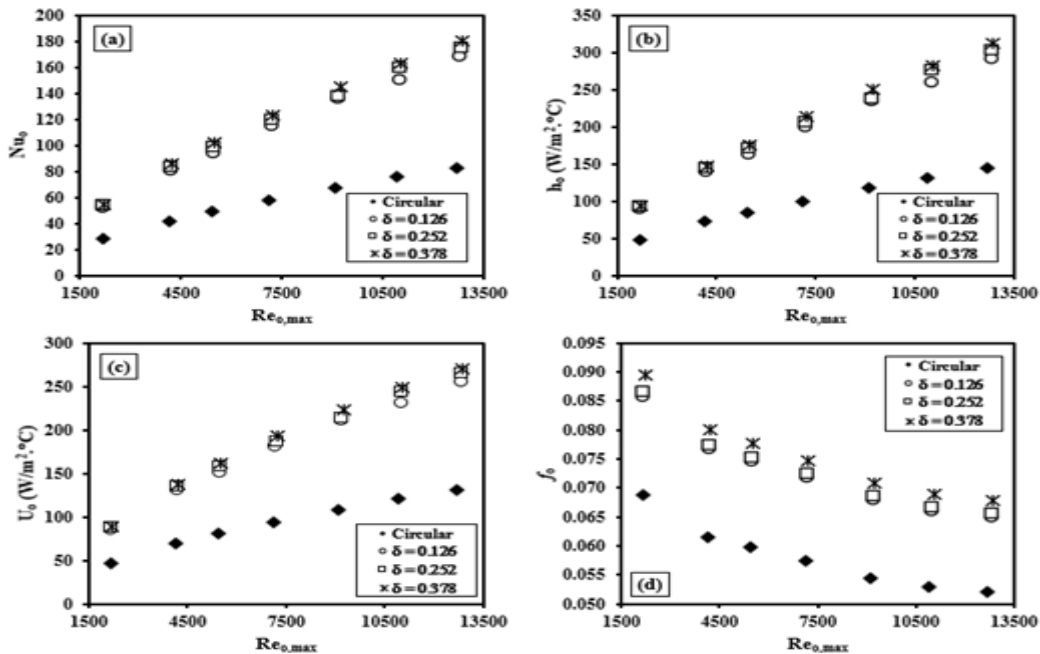


Fig. 6 Performance parameters at different bases-gaps ($S_T/d_{t,o} = S_L/d_{t,o} = 2.0$ and $\alpha = 60^\circ$); (a) \overline{Nu}_o , (b) \overline{h}_o , (c) U_o , (d) f_o .

6.2 Effect of The Spacing Between the Tubes in Transversal Direction

Here, three spaces in the transversal direction ($2 \leq S_T/d_{t,o} \leq 3$) are experienced for the inline setting and constant angle of the flow direction at 60° . A sample of the outputs for \overline{Nu}_o and f_o are presented in Fig. 7. The outputs assure that increasing the distance between the tubes in the transversal direction, from 2 to 3, decreases the \overline{Nu}_o and f_o by 27.3% and 39.8%, respectively. These drops may be due to weakness of the airflow strangling associated with growing the spacings between the tubes in the transversal direction, which weakens the flow impinging with the following tubes. This lessens the breaking of the airflow boundary layers, which accordingly deteriorates the cooling rate and the airflow resistance.

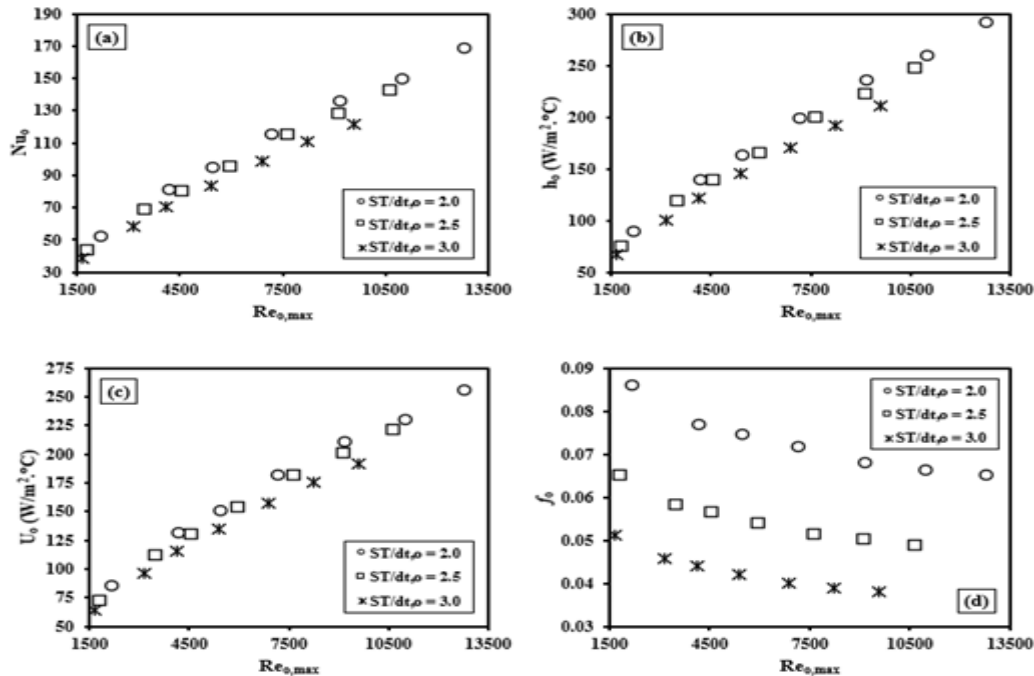


Fig. 7 Performance parameters at different transversal spacings ($S_L/d_{t,o} = 2.0$, $\alpha = 60^\circ$ and $\delta = 0.126$); (a) \overline{Nu}_o , (b) \overline{h}_o , (c) U_o , (d) f_o .

6.3 Effect of The Spacing Between the Tubes in Flow Direction

Here, three spaces in the longitudinal direction ($2 \leq S_L/d_{t,o} \leq 3$) are considered also for the aligned setting and fixed angle of the flow direction at 60° . Fig. 8 supplies a sample of the outputs for \overline{Nu}_o and f_o at $S_T/d_{t,o} = 3$ and $\delta = 0.378$ at different airflow rates. The results show that growing the longitudinal spacing ratio from 2 to 3 dampens the \overline{Nu}_o and f_o by 8% and 5.8%, respectively. These drops are due to weakening the impinging force of the air on the subsequent tubes. This weakens the turbulence level around the tubes, which diminishes the mixing between the fluid layers and between these layers and the adjacent tube surface. This consequently decreases both \overline{Nu}_o and f_o .

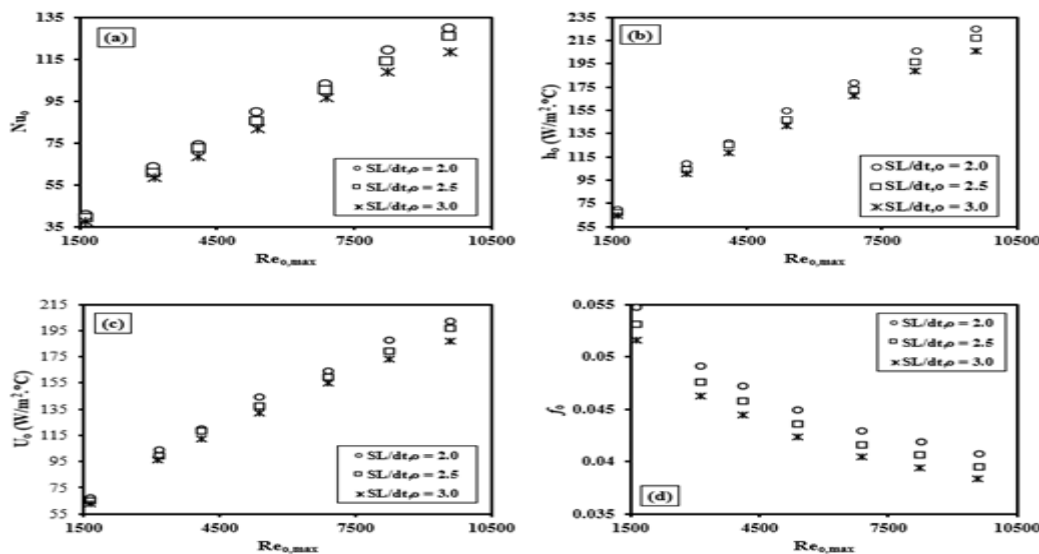


Fig. 8 Performance parameters at different longitudinal spacings ($S_T/d_{t,o} = 3.0$, $\alpha = 60^\circ$ and $\delta = 0.378$); (a) \overline{Nu}_o , (b) \overline{h}_o , (c) U_o , (d) f_o .

6.4 Hydrothermal Performance Approach

Several terminologies are recognized by other researchers to assess the performance attributes. In this work, the *HTPA* is presented by means of St_o and f_o ratios [30] estimated with engaging SCTs and CCT ones as heat transmission surfaces. It is clear from the findings that the *HTPA* is augmented by growing the gap between the flat bases in addition to growing the transversal and/or reducing longitudinal pitches. Also, there is a minor increase in the *HTPA* by growing the airflow rate.

$$HTPA = \frac{St_{o,SCT}/St_{o,CCT}}{(f_{o,SCT}/f_{o,CCT})^{1/3}} \quad (26)$$

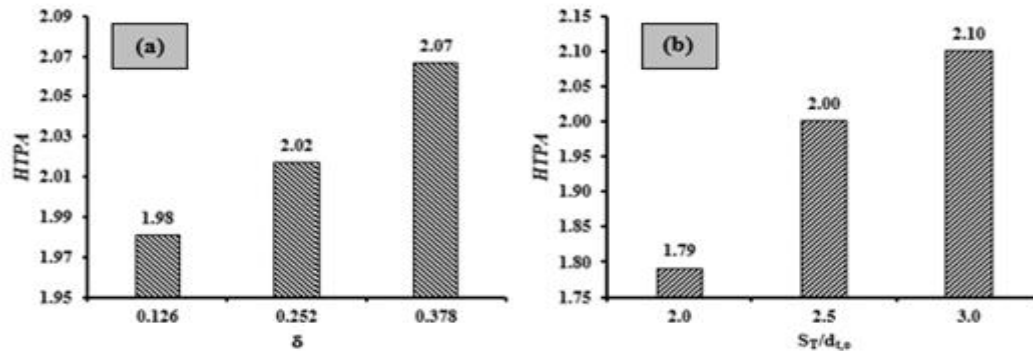


Fig. 9 The average *HTPI* versus; (a) δ , (b) $S_T/d_{t,o}$ ($\delta = 0.378$, $S_T/d_{t,o} = 3$, $S_L/d_{t,o} = 2$).

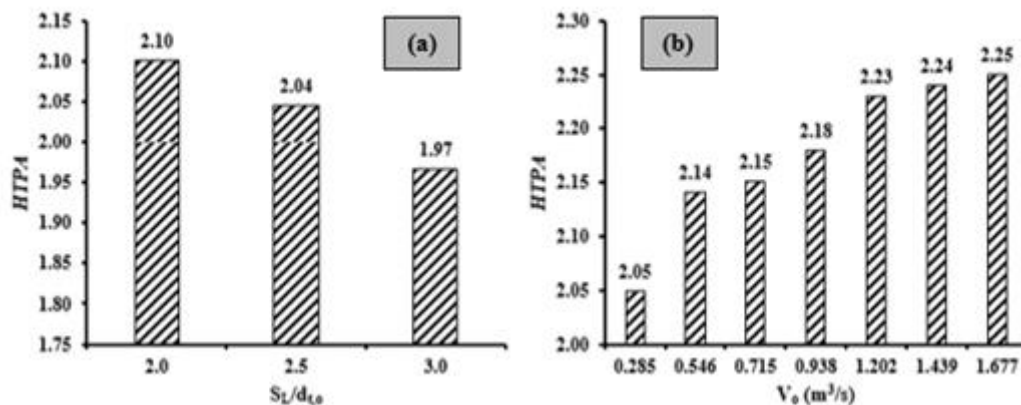


Fig. 10 The average *HTPI* versus; (a) $S_L/d_{t,o}$, (b) flow rate ($\delta = 0.378$, $S_T/d_{t,o} = 3$, $S_L/d_{t,o} = 2$).

7. Conclusions of the work

This work introduces an experimental examination of the hydrothermal characteristics of aligned CCT/SCT banks at an extensive extent of airflow rates across the tubes. During the tests, several gaps between SCTs-flat bases with different pitches in/normal to flow directions are considered. The results of this work are as follows:

- SCT is a good passive augmentation tool for the air-cooling load, but it indirectly requires an extra pumping power for the same flow rate.
- The \overline{Nu}_o and f_o are increased by increasing the gap between the SCTs-flat bases and decreasing the longitudinal and/or transversal pitches of the tubes.
- The *HTPA* is affected by varying SCT geometrical parameters. It is increased by:
 - increasing the space between the SCTs-flat bases.
 - increasing the transversal pitch ratio.
 - decreasing the longitudinal pitch ratio.
- The maximum verified value of *HTPA* is 2.25.

8. Appendix A

This section summarizes the equations applied to evaluate the uncertainties in all parameters as recognized by Kline and McClintock [31].

$$\frac{\omega_{\delta}}{\delta} = \pm \sqrt{\left(\frac{\omega_{S_b}}{S_b}\right)^2 + \left(\frac{-\omega_{d_{t,o}}}{d_{t,o}}\right)^2} = \pm \sqrt{\left(\frac{0.01}{2}\right)^2 + \left(\frac{-0.01}{15.88}\right)^2} = \pm 0.504\% \text{ (max. value)} \quad (27)$$

$$\frac{\omega_{S_T/d_{t,o}}}{S_T/d_{t,o}} = \pm \sqrt{\left(\frac{\omega_{S_T}}{S_T}\right)^2 + \left(\frac{-\omega_{d_{t,o}}}{d_{t,o}}\right)^2} = \pm \sqrt{\left(\frac{0.01}{23.81}\right)^2 + \left(\frac{-0.01}{15.88}\right)^2} = \pm 0.076\% \text{ (max. value)} \quad (28)$$

$$\frac{\omega_{S_L/d_{t,o}}}{S_L/d_{t,o}} = \pm \sqrt{\left(\frac{\omega_{S_L}}{S_L}\right)^2 + \left(\frac{-\omega_{d_{t,o}}}{d_{t,o}}\right)^2} = \pm \sqrt{\left(\frac{0.01}{23.81}\right)^2 + \left(\frac{-0.01}{15.88}\right)^2} = \pm 0.076\% \text{ (max. value)} \quad (29)$$

$$\omega_{S_T-d_{t,o}} = \pm \sqrt{(\omega_{S_T})^2 + (-\omega_{d_{t,o}})^2} = \pm \sqrt{(0.01)^2 + (-0.01)^2} = \pm 0.014 \text{ mm} \quad (30)$$

$$\frac{\omega_{A_{t,o}}}{A_{t,o}} = \pm \sqrt{\left(\frac{\omega_{d_{t,o}}}{d_{t,o}}\right)^2 + \left(\frac{\omega_{L_t}}{L_t}\right)^2} = \pm \sqrt{\left(\frac{0.01}{15.88}\right)^2 + \left(\frac{0.5}{950}\right)^2} = \pm 0.082\% \text{ (max. value)} \quad (31)$$

$$\frac{\omega_{A_{t,i}}}{A_{t,i}} = \pm \sqrt{\left(\frac{\omega_{d_{t,i}}}{d_{t,i}}\right)^2 + \left(\frac{\omega_{L_t}}{L_t}\right)^2} = \pm \sqrt{\left(\frac{0.01}{14.45}\right)^2 + \left(\frac{0.5}{950}\right)^2} = \pm 0.087\% \text{ (max. value)} \quad (32)$$

$$\frac{\omega_{A_{duct}}}{A_{bore}} = \pm \sqrt{\left(\frac{\omega_W}{W}\right)^2 + \left(\frac{\omega_H}{H}\right)^2} = \pm \sqrt{\left(\frac{0.5}{250}\right)^2 + \left(\frac{0.5}{950}\right)^2} = \pm 0.21\% \quad (33)$$

$$\frac{\omega_{A_{orifice}}}{A_{orifice}} = \pm \sqrt{\left(\frac{2\omega_{d_{orifice}}}{d_{orifice}}\right)^2} = \pm \left(\frac{2 * 0.5}{101.6}\right) = \pm 0.984\% \quad (34)$$

$$\omega_{\Delta T_w} = \pm \sqrt{(\omega_{T_{w,o}})^2 + (-\omega_{T_{w,i}})^2} = \pm 0.5 * \sqrt{2} = \pm 0.71^\circ\text{C} \quad (35)$$

$$\omega_{\Delta T_a} = \pm \sqrt{(\omega_{T_{a,i}})^2 + (-\omega_{T_{a,o}})^2} = \pm 0.04 * \sqrt{2} = \pm 0.06^\circ\text{C} \quad (36)$$

$$\omega_{\Delta T_i} = \omega_{\Delta T_o} = \pm \sqrt{(\omega_{T_{a,ave,i}})^2 + (-\omega_{T_{w,o}})^2} = \pm \sqrt{(0.04)^2 + (0.5)^2} \cong \pm 0.5^\circ\text{C} \quad (37)$$

$$\omega_{\Delta T_{L,M}} = \pm \frac{\omega_T \sqrt{2}}{\ln \left[\frac{\Delta T_i}{\Delta T_o} \right]} \sqrt{2 - 2\Delta T_{L,M} \left(\frac{1}{\Delta T_i} + \frac{1}{\Delta T_o} \right) + \Delta T_{L,M}^2 \left(\frac{1}{\Delta T_i^2} + \frac{1}{\Delta T_o^2} \right)} \quad (38)$$

$$\frac{\omega_{u_o}}{u_o} = \pm \sqrt{\left(\frac{0.7566 \omega_{\Delta H_{orifice}}}{\Delta H_{orifice}}\right)^2 + \left(\frac{\omega_{A_{duct}}}{A_{duct}}\right)^2 + \left(\frac{\omega_{A_{orifice}}}{A_{orifice}}\right)^2} \cong \pm 4.29\% \text{ (max. value)} \quad (39)$$

$$\frac{\omega_{u_{o,max}}}{u_{o,max}} = \pm \sqrt{\left(\frac{\omega_{u_o}}{u_o}\right)^2 + \left(\frac{\omega_{S_T}}{S_T}\right)^2 + \left(\frac{\omega_{S_T-d_{t,o}}}{S_T-d_{t,o}}\right)^2} \cong \pm 4.29\% \text{ (max. value)} \quad (40)$$

$$\frac{\omega_{Re_{o,max}}}{Re_{o,max}} = \pm \sqrt{\left(\frac{\omega_{u_{o,max}}}{u_{o,max}}\right)^2 + \left(\frac{\omega_{d_{t,o}}}{d_{t,o}}\right)^2 + \left(\frac{\omega_{v_o}}{v_o}\right)^2} \cong \pm 4.29\% \text{ (max. value)} \quad (41)$$

$$\frac{\omega_{\dot{V}_o}}{\dot{V}_o} = \pm \frac{0.7566 \omega_{\Delta H_{orifice}}}{\omega_{\Delta H_{orifice}}} = \pm 0.32\% \text{ (max. value)} \quad (42)$$

$$\frac{\omega_{\dot{m}_o}}{\dot{m}_o} = \pm \sqrt{\left(\frac{\omega_{\dot{V}_o}}{\dot{V}_o}\right)^2 + \left(\frac{\omega_{\rho_o}}{\rho_o}\right)^2} = \pm 0.33\% \text{ (max. value)} \quad (43)$$

$$\omega_{\dot{V}_w} = \pm \sqrt{\left(\frac{1}{1} * 0.01\right)^2 + \left(\frac{-50}{1^2} * \left(\frac{1}{60}\right)\right)^2} = \pm 0.83341/\text{min} = \frac{\pm 0.8334}{50} * 100 = \pm 1.67\% \quad (44)$$

$$\frac{\omega_{\dot{m}_w}}{\dot{m}_w} = \pm \sqrt{\left(\frac{\omega_{\rho_w}}{\rho_w}\right)^2 + \left(\frac{\omega_{\dot{V}_w}}{\dot{V}_w}\right)^2} = \pm \sqrt{(0.001)^2 + (0.0167)^2} = \pm 1.67\% \quad (45)$$

$$\frac{\omega_{Re_i}}{Re_i} = \pm \sqrt{\left(\frac{\omega_{\dot{m}_w}}{\dot{m}_w}\right)^2 + \left(\frac{\omega_{d_{t,h}}}{d_{t,h}}\right)^2 + \left(\frac{\omega_{\mu_i}}{\mu_i}\right)^2} \cong \pm 1.67\% \text{ (max. value)} \quad (46)$$

$$\frac{\omega_{Q_o}}{Q_o} = \pm \sqrt{\left(\frac{\omega_{\dot{m}_o}}{\dot{m}_o}\right)^2 + \left(\frac{\omega_{Cp_o}}{Cp_o}\right)^2 + \left(\frac{\omega_{\Delta T_a}}{\Delta T_a}\right)^2} \quad (47)$$

$$\frac{\omega_{Q_i}}{Q_i} = \pm \sqrt{\left(\frac{\omega_{\dot{m}_i}}{\dot{m}_i}\right)^2 + \left(\frac{\omega_{Cp_i}}{Cp_i}\right)^2 + \left(\frac{\omega_{\Delta T_w}}{\Delta T_w}\right)^2} \quad (48)$$

$$\omega_{Q_{ave}} = \pm \frac{1}{2} \sqrt{(\omega_{Q_o})^2 + (\omega_{Q_i})^2} \quad (49)$$

$$\frac{\omega_{U_o}}{U_o} = \pm \sqrt{\left(\frac{\omega_{Q_{ave}}}{Q_{ave}}\right)^2 + \left(\frac{-\omega_{A_{t,o}}}{A_{t,o}}\right)^2 + \left(\frac{-\omega_{\Delta T_{L,M}}}{\Delta T_{L,M}}\right)^2} \quad (50)$$

$$\frac{\omega_{\overline{Nu}_i}}{\overline{Nu}_i} = \pm \sqrt{\left(\frac{0.8 \omega_{Re_i}}{Re_i}\right)^2 + \left(\frac{0.4 \omega_{Pr_i}}{Pr_i}\right)^2} \cong \pm 1.34\% \text{ (max. value)} \quad (51)$$

$$\frac{\omega_{\bar{h}_i}}{\bar{h}_i} = \pm \sqrt{\left(\frac{\omega_{\bar{Nu}_i}}{\bar{Nu}_i}\right)^2 + \left(\frac{\omega_{k_i}}{k_i}\right)^2 + \left(\frac{-\omega_{d_{t,h}}}{d_{t,h}}\right)^2} \cong \pm 1.35\% \text{ (max. value)} \quad (52)$$

$$\omega_{\bar{h}_o} = \pm \sqrt{\left(\frac{\partial \bar{h}_o}{\partial U_o} \omega_{U_o}\right)^2 + \left(\frac{\partial \bar{h}_o}{\partial A_{t,o}} \omega_{A_{t,o}}\right)^2 + \left(\frac{\partial \bar{h}_o}{\partial A_{t,i}} \omega_{A_{t,i}}\right)^2 + \left(\frac{\partial \bar{h}_o}{\partial h_i} \omega_{\bar{h}_i}\right)^2} \quad (53)$$

$$\frac{\omega_{\bar{Nu}_o}}{\bar{Nu}_o} = \pm \sqrt{\left(\frac{\omega_{\bar{h}_o}}{\bar{h}_o}\right)^2 + \left(\frac{\omega_{d_{t,o}}}{d_{t,o}}\right)^2 + \left(\frac{-\omega_{k_o}}{k_o}\right)^2} \quad (54)$$

$$\frac{\omega_{St_o}}{St_o} = \pm \sqrt{\left(\frac{\omega_{\bar{Nu}_o}}{\bar{Nu}_o}\right)^2 + \left(\frac{\omega_{Re_{o,max}}}{Re_{o,max}}\right)^2 + \left(\frac{-\omega_{Pr_o}}{Pr_o}\right)^2} \quad (55)$$

$$\frac{\omega_{f_o}}{f_o} = \pm \sqrt{\left(\frac{\omega_{\Delta P_o}}{\Delta P_o}\right)^2 + \left(\frac{\omega_{\rho_o}}{\rho_o}\right)^2 + \left(\frac{-2\omega_{u_{o,max}}}{u_{o,max}}\right)^2} \quad (56)$$

$$\frac{\omega_{HTPI}}{HTPI} = \pm \sqrt{\left(\frac{\omega_{St_{o,SCT}}}{St_{o,SCT}}\right)^2 + \left(\frac{\omega_{St_{o,CCT}}}{St_{o,CCT}}\right)^2 + \left(\frac{\frac{1}{3}\omega_{f_{o,SCT}}}{f_{o,SCT}}\right)^2 + \left(\frac{\frac{1}{3}\omega_{f_{o,CCT}}}{f_{o,CCT}}\right)^2} \quad (57)$$

References

- [1] M.R. Salem, "Experimental investigation on the hydrothermal attributes of MWCNT/water nanofluid in the shell-side of shell and semi-circular tubes heat exchanger", *Applied Thermal Engineering*, vol. 176, Article no. 115438, 2020.
- [2] T.L. Bergman, A.S. Lavine, F.P. Incropera and D.P. Dewitt, "Fundamentals of Heat and Mass Transfer", 7th edition, John Wiley & Sons, 2011.
- [3] J.W. Baughn, M.J. Elderkin, A.A. McKillop, "Heat transfer from a single cylinder, cylinders in tandem, and cylinders in the entrance region of a tube bank with a uniform heat flux", *Journal of Heat Transfer*, vol. 108(2), pp. 386-391, 1986.
- [4] Y.H. Zhang, L.B. Wang, Y.X. Su, S.D. Gao, "Effects of the pitch of in-line delta winglet vortex generators on heat transfer of a finned three-row flat tube bank", *Experimental Heat Transfer*, vol. 17, pp. 69-90, 2004.
- [5] M. Moawed, "Thermal performance of a cross flow heat exchanger with semi-circular tubes", *ERJ Shoubra Faculty of Engineering*, vol. 4, pp. 87-109, June 2005.
- [6] S.A. Nada, H.El-Batsh, M. Moawed, "Heat transfer and fluid flow around semi-circular tube in cross flow at different orientations", *Heat Mass Transfer*, vol. 43, pp. 1157-1169, 2007.
- [7] H. Bayat, A.M. Lavasani, T. Maarefdoost, "Experimental study of thermal-hydraulic performance of cam-shaped tube bundle with staggered arrangement", *Energy Conversion and Management*, vol. 85, pp. 470-476.
- [8] X.B. Zhao, G.H. Tang, X.W. Ma, Y. Jin, W.Q. Tao, "Numerical investigation of heat transfer and erosion characteristics for H-type finned oval tube with longitudinal vortex generators and dimples", *Applied Energy*, vol. 127, pp. 93-104, 2014.
- [9] Y. He, H. Han, S. Tang, T. Zhou, "Sulfuric acid deposition characteristics of H-type finned tube bank with 10 rows", *International Journal of Heat and Mass Transfer*, vol. 81, pp. 137-141, 2015.
- [10] A. Yilmaz, T. Yilmaz, "Optimum design of cross-flow in-line tube banks at constant wall temperature", *Heat Transfer Engineering*, vol. 37(6), pp. 523-534, 2016.
- [11] A. Yilmaz, M.N. Kuru, M.T. Erdinç, T. Yilmaz, "Numerical calculation of heat transfer and pressure drop in inline axially finned tube banks", 1st International Mediterranean Science and Engineering Congress (IMSEC 2016), October 26-28, 2016, Adana/Turkey.
- [12] E. Martinez-Espinosa, W. Vicente, M. Salinas-Vazquez, I. Carvajal-Mariscal, "Numerical analysis of turbulent flow in a small helically segmented finned tube bank", *Heat Transfer Engineering*, vol. 38(1), pp. 47-62, 2017.
- [13] A.K. Mohanan, B.V. Prasad, S. Vengadesan, "Fluid flow and thermal performance in circular, elliptical and mixed tube bundle cross flow heat exchanger", *Twelve International Conference on Thermal Engineering: Theory and Applications*, February 23-26, 2019, Gandhinagar, India.
- [14] H.G. Ramírez-Hernández, F.A. Sánchez-Cruz, F.J. Solorio-Ordaz, S. Martínez-Martínez, "An experimental study of heat transfer on a tube bank under frost formation conditions", *International Journal of Refrigeration*, vol. 102, pp. 35-46, 2019.
- [15] P. Souza, D. Biswas, S.P. Deshmukh, "Air side performance of tube bank of an evaporator in a window air-conditioner by CFD simulation with different circular tubes with uniform transverse pitch variation", *International Journal of Thermofluids*, vol. 3-4, article no. 100028, 2020.
- [16] A. Choudhary, M. Kumar, A.K. Patil, S. Chamoli, "Enhanced thermal and fluid flow performance of cross flow tube bank with perforated splitter plate", *Experimental Heat Transfer*, 2020.
- [17] W. Zhong, X. Cao, Y. Yuan, "Optimization of falling film thermosyphons bundle arrangement for large-scale cooling applications by genetic algorithm", *Applied Thermal Engineering*, vol. 169, article no. 114892, 2020.
- [18] M.R. Salem, K.M. Elshazly, R.Y. Sakr, R.K. Ali, "Experimental study on convective heat transfer and pressure drop of water-based nanofluid inside shell and coil heat exchanger", PhD dissertation, Faculty of Engineering at Shoubra, Benha University, 2014.
- [19] M.R. Salem, M.B. Eltoukhey, R.K. Ali, K.M. Elshazly, "Experimental investigation on the hydrothermal performance of a double-pipe heat exchanger using helical tape insert", *International Journal of Thermal Sciences*, vol. 124, pp. 496-507, 2018.
- [20] K.M. Elshazly, R.Y. Sakr, R.K. Ali, M.R. Salem, "Effect of $\gamma\text{-Al}_2\text{O}_3$ /water nanofluid on the thermal performance of shell and coil heat exchanger with different coil torsions", *Heat and Mass Transfer*, vol. 53 (6), 1893-1903, 2017.

- [21] M.R. Salem, "Performance enhancement of a vapor compression refrigeration system using R134a/MWCNT-oil mixture and liquid-suction heat exchanger equipped with twisted tape turbulator", *International Journal of Refrigeration*, vol. 120, 357-369, 2020.
- [22] S.M. Elshamy, M.T. Abdelghany, M.R. Salem, O.E. Abdellatif, "Based Al₂O₃ nanofluid including diverse coil geometries: An experimental study", *Journal of Nanofluids*, vol. 9 (1), 13-23, 2020.
- [23] M.R. Salem, H.A. El-Gammal, A.A. Abd-Elaziz, K.M. Elshazly, "Study of the performance of a vapor compression refrigeration system using conically coiled tube-in-tube evaporator and condenser", *International Journal of Refrigeration*, vol. 99, 393-407, 2019.
- [24] H.A. Refaey, E. Specht, M.R. Salem, "Influence of fuel distribution and heat transfer on energy consumption in tunnel kilns", *International Journal of Advances in Engineering & Technology (IJAET)*, vol. 8(3), 281-293, 2015.
- [25] R.K. Shah, D.P. Sekulić, "Fundamentals of heat exchanger design", 6th edition, Hoboken, NJ: John Wiley & Sons, p. 189, 2003.
- [26] V. Gnielinski, "New equations for heat and mass transfer in turbulent pipe and channel flow", *International Chemical Engineering*, vol. 16, pp. 359-368, 1976.
- [27] G.K. Filonenko, "Hydraulic resistance of pipes (Hydraulischer Widerstand von Rohrleitungen)," *Teplotenergetika*, vol. 1(4), pp. 40-44, 1954.
- [28] A. Zukauskas, "Heat transfer from tubes in cross flow", in J.P. Hartnett and T.F. Irvine, Jr., Eds., *Advances in Heat Transfer*, vol. 8, Academic Press, New York, 1972.
- [29] M. Jakob, "Heat transfer and flow resistance in cross flow of gases over tube banks", *Trans. ASME*, vol. 60, p. 384, 1938.
- [30] H.H. Al-Kayiem, A. Bin Ekhwan, L.N. Muhi, "Augmentation of ribs turbulators height on the hydrothermal performance of double pipe heat exchanger", *Journal of Engineering Science and Technology*, vol. 12(2), pp. 548-563, 2017.
- [31] S.J. Kline, F.A. McClintock, "Describing uncertainties in single-sample experiments", *Mechanical Engineering*, vol. 75(1), pp. 3-8, 1953.